

# Brachistochrone curve of a fluid filled cylinder: Not too fast, not too slow

Srikanth Sarma Gurram<sup>1</sup>, Sharan Raja<sup>1</sup>, Mahesh V. Panchagnula<sup>2†</sup>  
and Pallab Sinha Mahapatra<sup>1</sup>

<sup>1</sup>Department of Mechanical Engineering, Indian Institute of Technology Madras, Chennai  
600036 India,

<sup>2</sup>Department of Applied Mechanics, Indian Institute of Technology Madras, Chennai 600036  
India

(Received xx; revised xx; accepted xx)

The brachistochrone curve for a non-dissipative particle tries to maximize inertia of the particle but for a fluid filled cylinder, increasing inertia would amount to increased dissipative losses. Hence the trade-off between inertia and dissipation plays a vital role in determining the brachistochrone curve of a fluid filled cylinder. This trade-off manifests itself in the form of an integro-differential equation governing the angular acceleration of the cylinder. Here, we compute the brachistochrone curve of a fluid filled cylinder using optimal control principles and investigate the effect of the aforementioned trade-off on the deviation of the brachistochrone curve from that of a non-dissipative particle. Also, we investigate the effects of the non-dimensional parameters of the problem on the shape of the brachistochrone curve. Finally, we analyze the stability of the time varying fluid flow in the cylinder and find an admissible region for the terminal point which would ensure the stability of the fluid flow as the cylinder rolls along the brachistochrone curve.

**Key words:** Optimal control, Dissipative dynamics, Brachistochrone, Droplet transport, Stability of time dependent flows

## 1. Introduction

In 1696, John Bernoulli posed a famous problem to the readers of *Acta Eruditorum Andre-Sohn (1696)*: "Given two points  $A$  and  $B$  in a vertical plane, what is the curve traced out by a point acted on only by gravity, which starts at  $A$  and reaches  $B$  in the shortest time?" This problem was the inception of calculus of variations and subsequently resulted in several engineering applications such as optimal control. We are interested in a fluid dynamic variant of that question. Most literature in optimal control deals with systems with state equations where the velocities at the current moment will be a function of only the current position and the current control action i.e, the time evolution of the system can be determined by just the current state and the future control actions. In the case of a fluid filled cylinder, the combined time evolution of the fluid and the cylinder can be determined if the current velocity information of the cylinder, the velocity field of the fluid flow and the future control actions are given. But, computing the flow field at each time step can become computationally intensive. By removing the velocity field of the fluid from explicitly appearing in the state equation of the cylinder, we end up with

† Email address for correspondence: mvp@iitm.ac.in

an equation which would need all of the past values of the cylinder velocities to compute the time evolution. This memory dependence of the system is what makes the fluid filled cylinder interesting. This property has been illustrated in [Supekar & Panchagnula \(2014\)](#) while discussing the dynamics of a fluid filled cylinder rolling down an inclined plane.

Over the years, the brachistochrone problem has been extended by many people like [Gemmer \*et al.\* \(2006\)](#) by introducing field varying gravity, [Lipp \(1997\)](#) by including coulomb friction and [Vratanar & Saje \(1998\)](#) by including non-conservative forces. Despite the long history of the brachistochrone problem, it has not been extended into fluid mechanics context except by modeling fluid effects empirically as done by [Lipp \(1997\)](#). Our work tries to close this gap in the literature by using the coupled equations of fluid mechanics and rigid body mechanics to find the brachistochrone curve of a fluid filled cylinder. [Mertaniemi \*et al.\* \(2011\)](#) demonstrate approaches for droplet transport on super-hydrophobic tracks using gravity or electrostatic forces as the driving force. The obtained brachistochrone curve can find applications in transporting liquid drops on a super-hydrophobic surface of very low contact angle hysteresis in the fastest time.

Since the fluid filled cylinder is governed by a non-linear system of equations, the solution to the brachistochrone problem for a fluid filled cylinder is bound to have multiple solutions. Hence, this raises the question of the stability of any particular solution. Only those solutions which are stable with respect to infinitesimal disturbances would be physically realizable. Similar arguments have been made by [Hoffman \(2005\)](#) in the context of determining the shape of a twisted elastic loop. It is clear that if the system destabilizes while following a particular solution to a variational problem, then the solution would not be a physically realizable optima. For our problem, the only source of non-linearity is the navier stokes equation governing the dynamics of the fluid inside the cylinder. Hence, analyzing the stability of the evolution of the fluid dynamics would suffice for determining the stability of the overall solution to the brachistochrone problem.

Intuition says that for both high viscosity and low viscosity limits of the fluid, we retrieve back cycloid as a brachistochrone curve. So, by Rolle's theorem, there must exist a viscosity value at which the deviation from cycloid is maximum. To quantify this, we define two metrics for the deviation from a cycloid, one being a geometric deviation and the other a kinematic deviation.

The question we would be answering in this paper is as follows:

*“Given two points A and B in a vertical plane, what is the curve traced out by the center of mass of a fluid filled cylinder acted only by gravity, who's center of mass starts at A and reaches B in the shortest time?”*

## 2. Problem formulation

The equations governing a fluid filled cylinder are the rigid body equations for the cylindrical shell, Navier Stokes for the fluid and boundary conditions coupling both these equations. In the following section, we derive the governing equations for the case of a fluid filled cylinder rolling down an arbitrary curve in x-y plane.

### 2.1. Governing equations

The Navier stokes equations for the fluid flow in the rotating frame of reference of the rolling cylinder are as follows:

$$-\frac{v^2}{r} = \dot{\Omega}R \cos(\theta - \gamma(t)) - g \sin(\theta) - \frac{\partial p}{\partial r} \quad (2.1a)$$

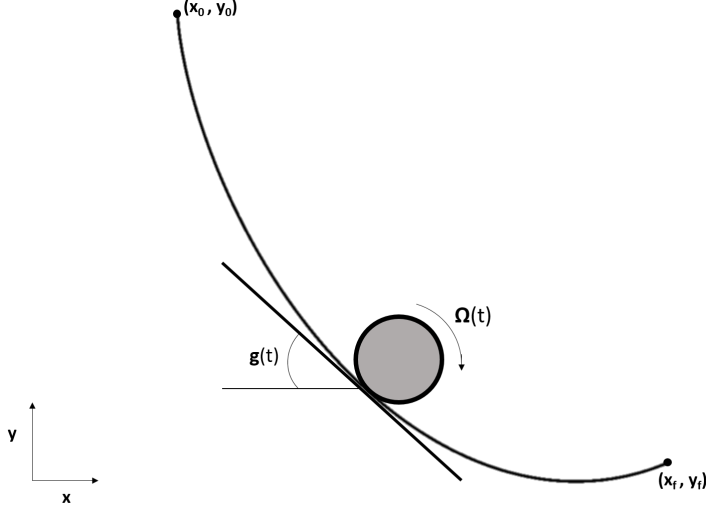


FIGURE 1. Schematic of the problem statement

$$\frac{\partial v}{\partial t} = -\dot{\Omega}R \sin(\theta - \gamma(t)) - g \cos(\theta) - \frac{1}{r} \frac{\partial p}{\partial \theta} + \nu \frac{\partial}{\partial r} \left( \frac{1}{r} \frac{\partial}{\partial r} (rv) \right) \quad (2.1b)$$

where,  $v$  is the azimuthal velocity with respect to the center of mass of the cylindrical shell,  $\gamma(t)$  is the inclination of the curved incline written in Lagrangian framework,  $\Omega(t)$  is the instantaneous angular velocity of the cylinder,  $g$  is the acceleration due to gravity,  $r$  and  $\theta$  are the normal polar coordinates. We can break down the pressure field  $p(r, \theta, t)$  as

$$p(r, \theta, t) = (\dot{\Omega}R \cos(\theta - \gamma(t)) - g \sin(\theta))r + p_d(r, t) \quad (2.2)$$

Substituting the above form of the pressure field will lead us to the following equation:

$$\frac{\partial v}{\partial t} = \nu \frac{\partial}{\partial r} \left( \frac{1}{r} \frac{\partial}{\partial r} (rv) \right) \quad (2.3)$$

The boundary conditions being:

$$v(R, t) = R\Omega(t) \quad (2.4a)$$

$$\frac{\partial v}{\partial r}(0, t) = 0 \quad (2.4b)$$

The rigid body equations for the cylinder are:

$$(m + M)R\dot{\Omega} = (m + M)g \sin \gamma(t) - f \quad (2.5a)$$

$$MR^2\dot{\Omega} = fR - T \quad (2.5b)$$

$$T(t) = 2\pi\mu R^2 h \left( \frac{\partial v}{\partial r} - \frac{v}{r} \right) \Big|_{r=R} \quad (2.6)$$

The cylinder would be starting from rest and the fluid would be quiescent. So,

$$\Omega(0) = 0 \quad \text{and} \quad v(0, r) = 0 \quad (2.7)$$

Now, we must look for a solution for the equations 2.3 to 2.7. Batchelor (2000) presents a closed form solution for Equation 2.3 with a constant boundary condition. But, here we have a time dependent boundary condition whose evolution is governed by the rigid body equations 2.5. Supekar & Panchagnula (2014) have extended the closed form solution of Batchelor (2000) to the case of a time varying boundary condition using duhammel's theorem and thereby, a solution was obtained for the case of a cylinder rolling down an inclined plane. We extend the same solution for our case by arguing that any curve in the x-y space is nothing but an inclined plane with it's inclination varying with space (or time in a Lagrangian framework). Using this solution, we can eliminate the equation 2.3 and be left with only equations 2.5 and 2.6. These equations lead to the following:

$$v(r, t) = \int_{\tau=0}^t \left( r + 2R \sum_{n=1}^{\infty} \frac{J_1(\lambda_n \frac{r}{R})}{\lambda_n J_0(\lambda_n)} \exp\left(-\lambda_n^2 \frac{\nu(t-\tau)}{R^2}\right) \right) \dot{\Omega}(\tau) d\tau \quad (2.8)$$

$$(m + 2M)R^2 \dot{\Omega}(t) = -T(t) + (m + M)gR \sin(\gamma(t)) \quad (2.9a)$$

$$T(t) = 4\pi\nu\rho R^2 h \sum_{n=1}^{\infty} \int_{\tau=0}^t \exp\left(-\lambda_n^2 \frac{\nu(t-\tau)}{R^2}\right) \dot{\Omega}(\tau) d\tau \quad (2.9b)$$

Where  $\lambda_n$  is the  $n^{th}$  root of the Bessel function of first kind. Now, we non-dimensionalize the above equations with  $\frac{R^2}{\nu}$  as the time scale,  $R$  as the length scale and  $\rho\pi R^2 h$  as the mass scale. As a result of this, we obtain two non-dimensional parameters:  $\pi_m = \frac{M}{\rho R^2 h}$  and  $\pi_g = \frac{gR^3}{\nu^2}$ . The resulting non-dimensional equations are:

$$(1 + 2\pi_m)\dot{\Omega}(t) = -4g(t) + (1 + \pi_m)\pi_g \sin(\gamma(t)) \quad (2.10)$$

where,

$$g(t) = \sum_{n=1}^{\infty} \int_{\tau=0}^t \exp(-\lambda_n^2(t-\tau)) \dot{\Omega}(\tau) d\tau \quad (2.11)$$

## 2.2. Optimization problem

We now formulate an optimization problem in the optimal control framework presented in Liberzon (2011). In this framework, the position  $(x(t), y(t))$  and angular velocity  $\Omega(t)$  of the cylinder comprise the state space of the cylinder and the inclination of the curve  $\gamma(t)$  will be the control action which controls the trajectory of the cylinder. Now, the problem is to find the control action  $\gamma(t)$  which will minimize the time of descent of the cylinder from a point A to point B. The kinematic equations of motion of the cylinder are:

$$\dot{x}(t) = \Omega(t) \cos(\gamma(t)) \quad (2.12)$$

$$\dot{y}(t) = -\Omega(t) \sin(\gamma(t)) \quad (2.13)$$

The optimization problem is now formulated as:

$$\text{Minimize}_{\gamma(t) \in [-\frac{\pi}{2}, \frac{\pi}{2}]} J(\gamma(t)) = \int_0^T dt \quad (2.14)$$

Such that:

$$\begin{aligned} x(0) &= x_0 & y(0) &= y_0 \\ x(T) &= x_f & y(T) &= y_f \end{aligned} \quad (2.15)$$

We use direct methods in optimal control to solve the optimization problem. For this, we discretize the equations 2.10 to 2.13 into  $N$  discrete equations each corresponding to  $N$  time steps. We use forward differencing scheme to generate the set of difference equations. For numerical reasons, we truncate the summation in equation 2.13 to finite number of terms. The difference equations obtained are as follows:

$$(1 + 2\pi_m)(\Omega[i + 1] - \Omega[i]) = -4g(i)\Delta t + (1 + \pi_m)\pi_g \sin(\gamma[i])\Delta t \quad (2.16)$$

$$x(i + 1) = x(i) + \Omega(i)\cos(\gamma(i))\Delta t \quad (2.17)$$

$$y(i + 1) = y(i) - \Omega(i)\sin(\gamma(i))\Delta t \quad (2.18)$$

$$g(i) = \sum_{j=1}^{i-1} \left( \sum_{k=1}^{n((i-j)\Delta t)} \exp(-\lambda_k^2(i-j)\Delta t) \right) (\Omega[j + 1] - \Omega[j]) \quad (2.19)$$

The truncation limit  $n((i-j)\Delta t)$  is chosen such that the addition of an extra term would not change the value of the sum by more than a threshold value ( $\sim 10^{-14}$ ). Simplifying the above equations, we get the following:

$$(1 + 2\pi_m)(\Omega[i + 1] - \Omega[i]) = -4 \sum_{j=1}^{i-1} (Coe f[i, j, \Delta t](\Omega[j + 1] - \Omega[j])\Delta t) + (1 + \pi_m)\pi_g \sin(\gamma[i])\Delta t \quad (2.20a)$$

$$Coe f[i, j, \Delta t] = \sum_{k=1}^{n[(i-j)\Delta t]} \exp(-\lambda_k^2(i-j)\Delta t) \quad (2.20b)$$

Equation 2.20 must be satisfied  $\forall i \in [1, N]$  while  $\Omega(1) = 0$ . The constraints on the terminal position of the cylinder obtained from equations 2.17 and 2.18 are as follows:

$$x_f = x_0 + \sum_{i=1}^N \Omega(i)\cos(\gamma(i))\Delta t \quad (2.21)$$

$$y_f = y_0 - \sum_{i=1}^N \Omega(i)\sin(\gamma(i))\Delta t \quad (2.22)$$

The resulting optimization problem becomes:

Minimize  $N \times \Delta t$  with equations 2.20, 2.21 and 2.22 as constraints.

### 3. Results

As discussed before, the deviation of a brachistochrone curve from cycloid is expected to be zero both at high and low viscosity ranges. There exists a particular  $\pi_g^*$  at which the deviation is maximum. The geometric deviation is defined as the following:

$$\delta = \int_{x_0}^{x_f} |y(x) - y_{cyc}(x)| dx \quad (3.1)$$

Where,

$\delta$  is the geometric deviation

$y(x)$  is the actual brachistochrone curve

$y_{cyc}(x)$  is the cycloid curve

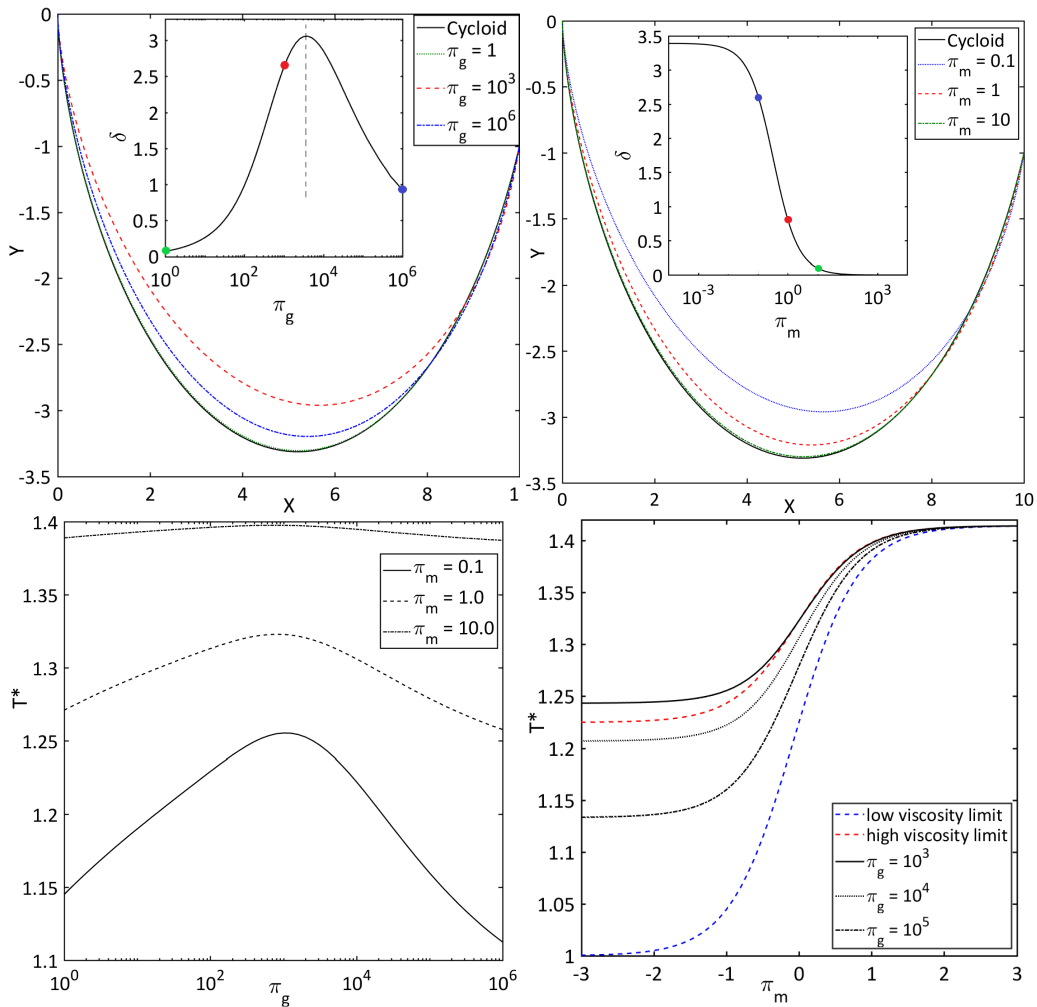


FIGURE 2. The figure shows the variation of brachistochrone curve with  $\pi_g$  at  $\pi_m = 0.1$  (top left) and with  $\pi_m$  at  $\pi_g = 1000$  (top right). The subplot inside each figure shows the geometric deviation  $\delta$  of the curve as a function of the parameters  $\pi_m$  and  $\pi_g$ . The locus of the peaks of the curve of  $\delta$  vs  $\pi_g$  for different  $\pi_m$  has been shown in the dotted lines in the subplot of the top left plot. The kinematic deviation plotted against  $\pi_g$  and  $\pi_m$  are shown in the in the bottom left and bottom right respectively.

The kinematic deviation is defined as the following:

$$T^* = \frac{T_{brac}}{T_{cyc}} \quad (3.2)$$

Where,

$T^*$  is the kinematic deviation

$T_{brac}$  is the total travel time of the fluid filled cylinder on the brachistochrone curve

$T_{cyc}$  is the time taken by a particle on a cycloid with same terminal point

The variation of the geometric deviation ( $\delta$ ) with respect to  $\pi_g$  shows a peak as expected. For the terminal point at  $(10, -1)$  and  $\pi_m = 0.1$ , the peak occurs at  $\pi_g \approx 3981$ . The

variation of the geometric deviation with respect to  $\pi_m$  shows a sigmoid-like behavior with an inflection point at  $\pi_m \approx 1$ . At low viscosity limit, the fluid filled cylinder is effectively a hoop with mass  $M$  and a point mass with mass  $m$  at the center. Where as, at high viscosity limit, the fluid filled cylinder acts like a hoop of mass  $M$  around a solid cylinder of mass  $m$ . So, at these two limits, dynamics of the fluid filled cylinder will boil down to rigid body dynamics which is the reason for the geometric deviation  $\delta$  to vanish at the high and low limits of viscosity. Also, at both low and high viscosity cases, the dissipation due to the fluid vanishes. The reasons being low viscosity coefficient and absence of velocity gradients respectively. This means that at both these limits, fluid filled cylinder will be faster than at other viscosity values. This fact can be verified from the plot on the bottom left figure 2. As the mass of fluid decreases i.e.,  $\pi_m$  increases, the effect of fluid will diminish leaving only the cylindrical shell. This is illustrated in the plot on the bottom left of figure 2 by the fact that the plot of kinematic deviation ( $T^*$ ) against  $\pi_g$  is becoming flatter at higher  $\pi_m$  values. The asymptotic value of  $T^*$  is square root of the ratio of the net inertial mass of a hoop to that of a particle. This turns out to be  $\sqrt{2}$ . Convergence to this limit is clearly seen in the bottom left plot of figure 2.

#### 4. Stability of fluid flow

In this section, we discuss the stability of the solution obtained by the framework mentioned in the previous section. All through the previous sections, we assume that flow field is governed by equation 2.8 and the viscous torque due to the fluid flow is as mentioned in 2.17. We now question this assumption and check for stability of the assumed flow field. As discussed before, the stability of the flow filed in turn speaks about the physical realizability of the solution to the brachistochrone problem.

##### 4.1. Linear stability equations

Since the navier stokes equations are the source of non-linearity in the system, we analyze the stability of the solution to the navier stokes equations as the fluid filled cylinder follows the brachistochrone curve. On linearizing the navier-stokes equations in polar coordinates and simplifying them with axisymmetric assumption and normal mode assumption of  $f(r, \theta, z, t) = \hat{f}(r, t) \exp(kz)$ , we obtain the following equations:

$$(DD^* - \alpha^2 - \frac{1}{\nu} \frac{\partial}{\partial t}) \hat{\psi} = \frac{2\alpha^2 V_b \hat{v}}{\nu r} \quad (4.1)$$

$$(DD^* - \alpha^2) \hat{u} = \hat{\psi} \quad (4.2)$$

$$(DD^* - \alpha^2 - \frac{1}{\nu} \frac{\partial}{\partial t}) \hat{v} = \frac{\hat{u} D^* V_b}{\nu} \quad (4.3)$$

Where,

$$D = \frac{\partial}{\partial r}$$

$$D^* = D + \frac{1}{r}$$

The equations 4.1 to 4.3 are scaled by using the using the same scaling law used before.

$$(DD^* - k^2 - \frac{\partial}{\partial t})\hat{\Psi} = \frac{2k^2V_b\hat{v}}{r} \quad (4.4)$$

$$(DD^* - k^2)\hat{u} = \hat{\Psi} \quad (4.5)$$

$$(DD^* - k^2 - \frac{\partial}{\partial t})\hat{v} = \hat{u}D^*V_b \quad (4.6)$$

The boundary conditions for 4.4 to 4.6 are as follows:

$$\left. \begin{aligned} \hat{u}(1, t) = \hat{v}(1, t) = D^*\hat{u}(1, t) = 0 \\ \hat{u}(0, t) = \hat{v}(0, t) = D^*\hat{u}(0, t) = 0 \\ \hat{\Psi}(1, t) = \frac{\partial^2 \hat{u}}{\partial r^2}(1, t) \\ \hat{\Psi}(0, t) = \frac{\partial^2 \hat{u}}{\partial r^2}(0, t) \end{aligned} \right\} \quad (4.7)$$

#### 4.2. Solution to the linear stability equations

To solve for the linear stability equations 4.4 to 4.7 and comment on the stability of the fluid flow, we adopt the same methodology used by [Chen & Kirchner \(1971\)](#) with slight modifications. The idea is to give an initial perturbation to the time varying flow and let it decay as long as the flow is stable. When the flow becomes unstable, the perturbation starts to grow. The instant when the growth begins is the point of instability. For numerical reasons, we spike the perturbation energy whenever it falls below a threshold. This is done so that the perturbation energy doesn't decay to a value lower than machine precision. We discretize the equations 4.4 to 4.7 using finite difference method and solve the resulting system of linear equations. To quantify the growth or decay of perturbations, we use the perturbation energy as a metric. The scaled version of perturbation energy as given below is used for this purpose:

$$E_p = \pi \int_0^1 r \left[ \hat{u}^2 + \hat{v}^2 + \frac{1}{k^2}(D^*\hat{u})^2 \right] dr \quad (4.8)$$

#### 4.3. Linear stability for the case of a brachistochrone fluid filled cylinder

Intuition tells us that if the terminal point of the brachistochrone curve is farther below the initial point, the flow is likely to become unstable even before it reaches the terminal point. Whereas, if the terminal point is vertically closer to the initial point, the flow is likely to remain stable till it reaches the terminal point. So, there would exist a boundary separating terminal points with completely stable fluid flow and those which will lead to an instability before reaching the terminal point. The following exercise is an attempt at capturing this boundary. The figure 3 shows this exercise of finding the stable and unstable terminal points.

Clearly from the figure 3 the plot on the right top is stable because there is no point at which the perturbation energy grows whereas the plot on the right bottom shows exponential growth in perturbation energy. So, this brachistochrone curve would be marked as unstable. This exercise of determining the stability of the fluid flow qualifies our framework of using laminar assumption to only a certain class of terminal points. Nevertheless,  $\pi_g$  and  $\pi_m$  of values as low as 0.1 are expected to appear in droplet transport problems mentioned by [Mertaniemi et al. \(2011\)](#). Hence, in this context, brachistochrone curve for a class of terminal points (stable) shown in green in figure 3 can be determined by assuming a laminar flow.

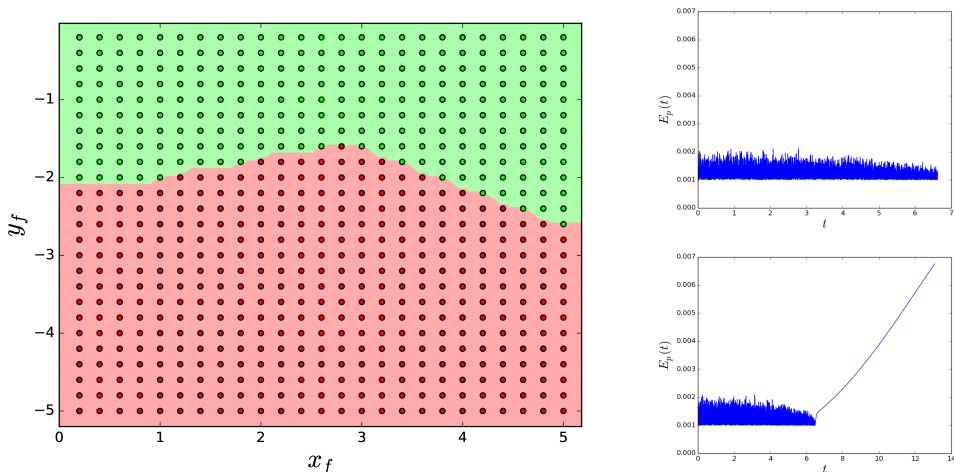


FIGURE 3. The figure shows the stable (in green) and unstable (in red) terminal points and the approximate stability margin (in black) for  $\pi_m = 0.1$  and  $\pi_g = 0.1$ . For every case, the first occurrence of instability is at  $k \rightarrow 0$ . The plot on the top right shows the perturbation energy of a stable brachistochrone curve ( $x_f = 0.6$ ,  $y_f = -1.6$ ) and the plot on the bottom right shows that for an unstable brachistochrone curve ( $x_f = 4.2$ ,  $y_f = -4.8$ ) both at  $\pi_m = 0.1$  and  $\pi_g = 0.1$

## 5. Discussion

For a wide range of terminal points, we find that the maximum deviation from a cycloid occurs at a parameter regime of  $\pi_g \approx 10^3$ . Also, we find that the effects of fluid on the deviation from a cycloid are significant only when  $\pi_m < 1$  i.e., the fluid mass is greater than the mass of the cylindrical shell. Hence, for parameter values of  $\pi_m > 1$  and  $\pi_g$  away from  $10^3$ , the brachistochrone curve can be approximated by a cycloid. For other parameter values, the framework provided in the problem formulation section can be used to compute the brachistochrone curve.

By analyzing the stability of brachistochrone curves for different  $\pi_m$  and  $\pi_g$ , we understand that for higher values of  $\pi_g$  the stable region shrinks. As a physical example, we see that for an Aluminum ( $\rho = 2700 \text{ kg/m}^3$ ) beverage can of radius 3 cm, height 10 cm and thickness 0.5 mm filled with silicone oil ( $\rho = 975 \text{ kg/m}^3$ ) of viscosity 5000 cSt, the non-dimensional quantities  $\pi_m$  and  $\pi_g$  are approximately equal to 0.1 and 10 respectively. The brachistochrone curve for this Aluminum can with end points at  $x = 30$  cm and  $y = -3$  cm will deviate significantly from the classic cycloid with the laminar flow inside it being stable.

The limit of  $\pi_m \rightarrow 0$  is a fair approximation of a cylindrical fluid liquid drop rolling down a super-hydrophobic surface. Since the deviation from cycloid at this limit is significantly high, the framework described here provides a way to compute the brachistochrone curve for a cylindrical fluid drop on a super-hydrophobic surface by neglecting the cylinder deformation.

## Appendix A.

In this appendix, we'll provide a brief mathematical derivation of the brachistochrone curve for the asymptotic cases of the fluid filled cylinder. Since the scales for non-

dimensionalization won't hold at these asymptotes, we go back to the dimensional form of the governing equations given in equations 2.8 and 2.9.

**Case 1:**

Consider the case where  $\nu \rightarrow 0$ . In non-dimensional terms, it means  $\pi_g \rightarrow \infty$ . In this case, equations 2.9 become:

$$\lim_{\nu \rightarrow 0} T(t) = 4\pi\rho R^2 h \sum_{n=1}^{\infty} \int_{\tau=0}^t \lim_{\nu \rightarrow 0} \nu \exp\left(-\lambda_n^2 \frac{\nu(t-\tau)}{R^2}\right) \dot{\Omega}(\tau) d\tau \quad (\text{A } 1)$$

$$\lim_{x \rightarrow 0} x \exp(-ax) = 0 \quad \forall a \in \mathbb{R} \quad (\text{A } 2)$$

Hence,

$$\lim_{\nu \rightarrow 0} T(t) = 0 \quad (\text{A } 3)$$

At this limit, the fluid inside doesn't rotate but just slips against the wall of the cylinder. This is shown by the fact that the rotational velocity of the fluid inside the cylinder vanishes at every radial location:

$$\lim_{\nu \rightarrow 0} v(r, t) = \int_{\tau=0}^t \left( r + 2R \sum_{n=1}^{\infty} \frac{J_1\left(\lambda_n \frac{r}{R}\right)}{\lambda_n J_0(\lambda_n)} \lim_{\nu \rightarrow 0} \exp\left(-\lambda_n^2 \frac{\nu(t-\tau)}{R^2}\right) \right) \dot{\Omega}(\tau) d\tau \quad (\text{A } 4)$$

$$\lim_{\nu \rightarrow 0} v(r, t) = \int_{\tau=0}^t \left( r + 2R \sum_{n=1}^{\infty} \frac{J_1\left(\lambda_n \frac{r}{R}\right)}{\lambda_n J_0(\lambda_n)} \right) \dot{\Omega}(\tau) d\tau \quad (\text{A } 5)$$

On computing the integrand explicitly using Mathematica, we find that the integrand converges to zero. Hence, the velocity field vanishes at each radial location at all times.

$$\lim_{\nu \rightarrow 0} v(r, t) = 0 \quad (\text{A } 6)$$

For the corresponding non-dimensional regime of  $\pi_g \rightarrow \infty$ , the torque applied by the fluid on the cylindrical shell vanishes. Since the fluid is just slipping against the rotating cylinder, the fluid is equivalent to a point mass at the center of the cylinder. Hence, at this limit, the fluid filled cylinder is effectively a hoop of mass  $M = \pi_m$  with a point mass of mass  $m = 1$  at the center.

**Case 2:**

Consider the case where  $\nu \rightarrow \infty$ . In non-dimensional terms, it means  $\pi_g \rightarrow 0$ . In this case, equations 2.9 become:

$$\lim_{\nu \rightarrow \infty} T(t) = 4\pi\rho R^2 h \sum_{n=1}^{\infty} \int_{\tau=0}^t \lim_{\nu \rightarrow \infty} \nu \exp\left(-\lambda_n^2 \frac{\nu(t-\tau)}{R^2}\right) \dot{\Omega}(\tau) d\tau \quad (\text{A } 7)$$

$$\lim_{x \rightarrow \infty} x \exp(-ax) = 0 \quad \forall a > 0 \quad (\text{A } 8)$$

Hence,

$$\lim_{\nu \rightarrow \infty} T(t) = 0 \quad (\text{A } 9)$$

Therefore, for the corresponding non-dimensional regime of  $\pi_g \rightarrow \infty$ , the torque applied by the fluid on the cylindrical shell vanishes. Unlike for the previous case, it isn't because of slipping of fluid against the cylinder. Here, it is because the fluid takes infinitesimally low transient time to reach the saturated velocity profile as shown below:

$$\lim_{\nu \rightarrow \infty} v(r, t) = \int_{\tau=0}^t \left( r + 2R \sum_{n=1}^{\infty} \frac{J_1\left(\lambda_n \frac{r}{R}\right)}{\lambda_n J_0(\lambda_n)} \lim_{\nu \rightarrow \infty} \exp\left(-\lambda_n^2 \frac{\nu(t-\tau)}{R^2}\right) \right) \dot{\Omega}(\tau) d\tau \quad (\text{A } 10)$$

From equation A 8,

$$\lim_{\nu \rightarrow \infty} v(r, t) = r\Omega(t) \quad (\text{A } 11)$$

Therefore, the fluid is undergoing a rigid body rotation. Hence, at this limit, the fluid filled cylinder is equivalent to a hoop of mass  $M = \pi_m$  and a solid cylinder of mass  $m = 1$ .

### Brachistochrone curve for a general rigid body:

Consider a rolling rigid body with a radius of gyration of  $k$  and mass  $M_b$ . Now, the brachistochrone curve for this rigid body is governed by the following variational formulation:

$$\text{Minimize}_{y(x) \in \mathbb{C}(\mathbb{R})} \sqrt{1 + \frac{k^2}{R^2}} \int_0^{x_f} \sqrt{\frac{1+y'^2}{2gy}} dx \quad (\text{A } 12)$$

Since the functional is just a scalar multiple of that for a particle, the solution for the above variational problem is also a cycloid. Hence, for any rolling rigid body, for a minimum time travel under gravity, the center of mass must follow a cycloid.

Both the cases discussed earlier result in finding the brachistochrone curve of different rigid bodies. So, these cases lead to a brachistochrone curve of a cycloid. Hence, at these asymptotes, the deviation from a cycloid vanishes. Also, for the general rigid body discussed above, the ratio of acceleration of the rigid body to that of a particle while on a cycloid curve is given by  $1/(1 + \frac{k^2}{R^2})$ . Hence the ratio of time of descent i.e., the kinematic deviation( $T^*$ ) as defined in 3.2 becomes  $\sqrt{1 + \frac{k^2}{R^2}}$ . The radius of gyration for cases 1 and 2 discussed earlier are  $k_1 = \sqrt{\frac{\pi_m}{1+\pi_m}}R$  and  $k_2 = \sqrt{\frac{1+2\pi_m}{2(1+\pi_m)}}R$ . This explains the asymptotic limits in the plot of  $T^*$  vs  $\pi_m$  as shown in the bottom right of figure 2. Also, for the case of  $\pi_m \rightarrow \infty$ , the fluid filled cylinder is effectively a hoop of mass  $\pi_m$  with negligible mass of fluid. Hence, the radius of gyration of the effective rigid body is  $k = R$ . This means that the kinematic deviation tends towards  $\sqrt{2}$ . This verifies the plot on the bottom left of the figure 2.

## REFERENCES

- ANDRE-SOHN, E. 1696 *Acta Eruditorum: Anno ... publicata. 1696*. Georgius.
- BATCHELOR, G. K. 2000 *An Introduction to Fluid Dynamics*. Cambridge University Press.
- CHEN, C. F. & KIRCHNER, R. P. 1971 Stability of time-dependent rotational couette flow part 2. stability analysis. *Journal of Fluid Mechanics* **48** (2), 365384.
- GEMMER, J., UMBLE, R. & NOLAN, M. 2006 Generalizations of the Brachistochrone Problem. *ArXiv Mathematical Physics e-prints*, arXiv: math-ph/0612052.
- HOFFMAN, KATHLEEN A. 2005 Stability results for constrained calculus of variations problems: An analysis of the twisted elastic loop. *Proceedings: Mathematical, Physical and Engineering Sciences* **461** (2057), 1357–1381.
- LIBERZON, DANIEL 2011 *Calculus of Variations and Optimal Control Theory: A Concise Introduction*. Princeton, NJ, USA: Princeton University Press.
- LIPP, STEPHEN C. 1997 Brachistochrone with coulomb friction. *SIAM Journal on Control and Optimization* **35** (2), 562–584, arXiv: <https://doi.org/10.1137/S0363012995287957>.
- MERTANIEMI, HENRIKKI, JOKINEN, VILLE, SAINIEMI, LAURI, FRANSSILA, SAMI, MARMUR,

- ABRAHAM, IKKALA, OLLI & RAS, ROBIN HA 2011 Superhydrophobic tracks for low-friction, guided transport of water droplets. *Advanced Materials* **23** (26), 2911–2914.
- SUPEKAR, ROHIT B & PANCHAGNULA, MAHESH V 2014 Dynamics and stability of a fluid filled cylinder rolling on an inclined plane. *arXiv preprint arXiv:1408.6654* .
- VRATANAR, B. & SAJE, M. 1998 On the analytical solution of the brachistochrone problem in a non-conservative field. *International Journal of Non-Linear Mechanics* **33** (3), 489 – 505.